



# Development of a New Rockbolt with High Load and Large Deformation Capacities

Zhengming Yang<sup>1</sup> · Shuai Xu<sup>1</sup> · Hao Zhang<sup>1</sup> · Wenzhi Guo<sup>1</sup> · Ming Cai<sup>1,2,3</sup> 

Received: 3 February 2023 / Accepted: 31 May 2023 / Published online: 17 June 2023  
© The Author(s), under exclusive licence to Springer-Verlag GmbH Austria, part of Springer Nature 2023

## Abstract

A new rockbolt for rock support in deep underground engineering is developed. The bolt, which is called 2S-bolt, is composed of a threadbar, a sliding piston, a sliding-resistance cone pipe, an anchorage section, a plate, and a plate-nut. The deformation of the bolt is composed of frictional sliding of the sliding piston in the sliding-resistance cone pipe in the first deformation stage and steel stretching of the threadbar in the second deformation stage. The structure and working principle of the new bolt is introduced first, followed by a laboratory study of the sliding resistances of each component of the bolt. Next, laboratory static pull-out tests of 2S-bolts with different sliding piston lengths are conducted and the results analyzed. The test results show that the bolt with a 30 cm long sliding piston can increase the load from 120 kN in the first deformation stage to 210 kN in the second deformation stage and it has a deformation capacity and an energy absorption capacity of 500 mm and 83.5 kJ, respectively. The average anchor force of the bolt with a 45 cm long sliding piston is 181.7 kN with an energy absorption capacity of 77.8 kJ. When utilized for rock support in rockbursting and squeezing grounds, the newly developed 2S-bolt can absorb a large amount of energy at a higher load capacity.

## Highlights

- A new rockbolt called 2S-bolt is developed for rock support in deep underground engineering.
- The deformation of the 2S-bolt is composed of two stages: frictional sliding and steel stretching.
- The 2S-bolt uses a sliding piston and a conical tube to maintain high load resistance during sliding.
- Laboratory tests show that the 2S-bolt can increase load capacity, have large deformation and energy absorption capacities, and is suitable for use in squeezing and rockbursting grounds.

**Keywords** 2S-bolt · Self-swelling agent · High load and large deformation · High energy absorption

## 1 Introduction

The depths of some mines in China, Canada, Australia and South Africa have exceeded 2000 m. Some underground civil engineering projects, such as water diversion hydro-power and traffic tunnels have also exceeded the 2000 m depth (Dai et al. 2021; Kaiser and Cai 2012). In these deep underground excavations, the strain energy stored in the rock mass is high, which can lead to engineering challenges such as extensive spalling, rockburst and large deformation (Ansell 2005; Cai and Kaiser 2018; Ortlepp 2000). These events can threaten the safety of workers and equipment, increase the cost of mineral exploitation and underground construction as well as investment risk (Cai 2019). For safe and cost-effective underground construction and mining, it

✉ Ming Cai  
mcai@laurentian.ca

<sup>1</sup> Key Laboratory of Ministry of Education on Safe Mining of Deep Metal Mines, Northeastern University, Shenyang 110819, People's Republic of China

<sup>2</sup> School of Engineering and Computer Science, Laurentian University, Sudbury, ON, Canada

<sup>3</sup> MIRARCO, Laurentian University, Sudbury, ON, Canada

is important to apply engineering measures to prevent and control those geotechnical risks.

Rock support is an important tool to ensure excavation stability and prevent rock fall accident in mining. Traditional rock bolting technologies are not effective to ensure stability of mine excavations in highly stressed grounds (Kang et al. 2013; Li 2010). For example, fully grouted rebars using either resin or cement mortar grout are stiff and they do not have sufficient deformation capacity (Khaleghparast et al. 2023), which means that they can break and fail easily when the deformation is large (Hoek et al. 1995; Li and Doucet 2012; Srivastava and Singh 2015). End-anchored bolts such as mechanical bolts have a short anchorage section and a long free-deformation section, which means that they cannot reinforce a rock mass effectively. Split-sets have low pull-out and shear resistant capacities, which means that they are not suitable for ground control in high stress environments.

An ideal rockbolt should have a high load capacity and a large deformation capacity (Windsor and Thompson 1992). Conebolt (Jager 1992), which consists of a smooth steel bar and a conical head, can absorb energy as the cone slide through the grout; it is considered as the first energy-absorbing or yielding bolt for rock support in burst-prone grounds (Li et al. 2023). Since the development of conebolt, a few dozens of energy-absorbing rockbolts have been developed, which can be divided into three types based on their energy consumption mechanism: friction-sliding bolts, yielding-device bolts and steel-stretching bolts (Cai and Kaiser 2022).

A friction-sliding bolt absorbs energy by frictional sliding. Slip resistance is provided by friction between the bolt body and the borehole wall or grout or an energy-absorption section, and the bolt can maintain roughly a steady resistance during the deformation process. The load capacity of this type of bolt is usually lower than the yield load of the bolt's body; however, the deformation capacity is large. Typical friction-sliding bolts include Split-sets, Conebolt, MCB33 (Cai and Champaigne 2012), Roofex (Masoudi and Sharifzadeh 2018), Durabar (Ortlepp 2000), and He-bolt (He et al. 2014). A yielding-device bolt absorbs energy by deforming through or using a yielding device. Typical yielding-device bolts include Garford solid bar (Varden et al. 2008), cold drawing bolt (Wang et al. 2013), and AIEA-T bolt (Dai et al. 2018). A steel-stretching bolt absorbs energy by plastic deformation of the steel. The load capacity of this type of bolt is typically above the yield load of the bolt's body and the deformation capacity is governed by the elongation of the steel. Typical steel-stretching bolts include D-bolt (Li and Doucet 2012), Versa-Superbolt (Cai et al. 2019), and Par1 bolt (Knox and Berghorst 2019).

Among the existing energy-absorbing bolts, some have a low load capacity, some have a low deformation capacity, and some of the high energy-absorbing bolts have a high price tag. Therefore, the development of a high capacity

energy-absorbing bolt with reliable performance, low cost, high load and large deformation capacities is warranted for mining at depth.

This paper presents a new dynamic bolt called 2S-bolt that has high load and large deformation capacities. Firstly, we introduce the design of the new bolt, analyze the working principle of the bolt, and measure the slip resistance force of each component of the bolt. Secondly, static pull-out tests of the new bolt in different configurations are conducted to obtain the mechanical behaviors of the bolt. Finally, the mechanical properties of the new bolt are compared with some other energy-absorbing bolts and a cost analysis is conducted for the new bolt.

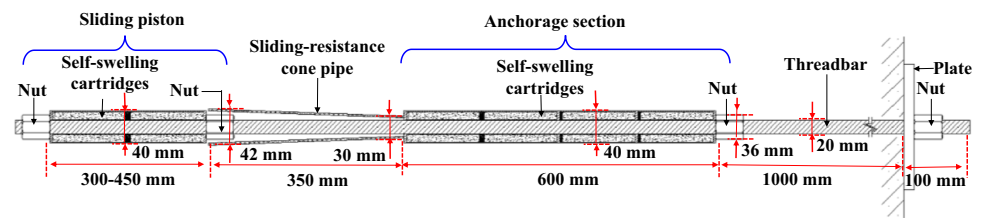
## 2 Structure and Energy Absorption Mechanism of 2S-Bolt

### 2.1 Structure of 2S-Bolt

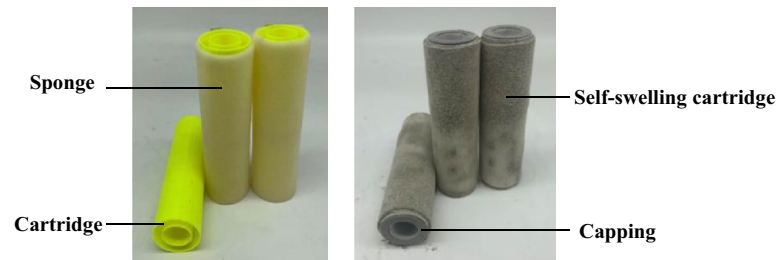
As shown in Fig. 1a, a 2S bolt is made using a threadbar with a sliding piston, a sliding-resistance cone pipe, an anchorage section, a plate, and a nut. The sliding piston is composed of self-swelling cartridges and two nuts that restrain both ends of the cartridges. The anchorage section is also composed of self-swelling cartridges and a nut that is located about 1 m from the plate to fix the self-swelling cartridges and to prevent them from slipping during bolt installation. The self-swelling cartridges used in the sliding piston and the anchorage sections are cylindrical hollow cartridges, which are filled with a self-swelling anchorage agent with a constant density. The outer wall of the hollow cartridge is made of plastics. As shown in Fig. 1b, water absorption holes and a cylindrical water absorption sponge are included to ensure sufficient water absorption of the anchorage agent. The self-swelling anchorage agent (Xu et al. 2021) expands after absorbing water to form a dense and hard calcium hydroxide compound that produces a large radial pressure in a confined space, which can increase the pressures between the anchorage agent and the borehole wall, thus increasing the frictional resistance of the anchorage agent. As shown in Fig. 1a, c, the sliding-resistance cone pipe is made of a seamless cone tube with a length of 350 mm, with outer diameters of 42 and 30 mm on the larger and smaller sides of the cone, respectively. The inner bolt of the 2S-bolt is a 20 mm diameter threadbar as shown in Fig. 1d, and hexagonal nuts that match the thread of the threadbar are used. One assembled 2S-bolt is presented in Fig. 1e.

The anchorage section of the 2S-bolt is tightly anchored with the rock after the completion of radial expansion of the anchorage agent and it will not slide when the load of the bolt is below a set threshold. However, the threadbar can be pulled out of the anchorage section when the load is above

**Fig. 1** 2S-bolt: **a** schematic diagram; **b** self-swelling cartridges; **c** sliding-resistance cone pipe; **d** threadbar and nut; **e** a sample of assembled 2S-bolt



(a)



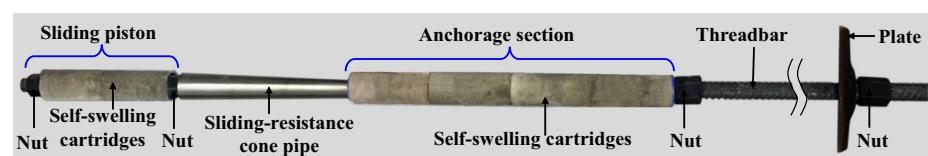
(b)



(c)



(d)



(e)

the threshold. Because both ends of the sliding piston are installed with nuts, the threadbar and the sliding piston will move in unison when the threadbar slides.

During the assembly of a 2S-bolt, the nut on the right of the anchorage section is installed first (Fig. 1e). The anchorage section is loaded with the self-swelling cartridges and then the sliding-resistance cone pipe is installed. Finally, the sliding piston is installed and the two ends are fixed by two nuts, as shown in Fig. 1e. Prior to installation of the bolt into a borehole, the assembled 2S-bolt is immersed in water for 8–12 min or sprayed with water for 12–15 min. After

the self-swelling anchorage agent is saturated with water, the bolt is inserted into the borehole, and the plate and the nut are installed. 30–120 min after installation, depending on the ambient temperature and humidity, the self-swelling anchorage agent begins to expand, forming a compacted and hard compound within the confined space of the borehole (Xu et al. 2021). The expansion of the agent generates a high pressure that increases the frictional resistance between the compound and the borehole wall. When an 2S-bolt is installed into an upwards borehole, a mechanical anchoring

head can be added to the bolt to provide the initial anchor force.

## 2.2 Energy Absorption Mechanism of 2S-Bolt

The deformation of an 2S-bolt under loading is shown schematically in Fig. 2. According to the deformation state of the bolt, the movement of the 2S-bolt and the rock mass can be divided into three stages.

Figure 2a shows the load build-up stage when the rock mass deforms initially. The tensile force is small and the threadbar is in the elastic deformation state. The self-swelling cartridges in the anchorage section are subjected mainly to a compressive stress and the anchor force is generated by the friction between the self-swelling cartridges and the threadbar. The bolt force is lower than the yield load of the threadbar; it is also lower than the force which will break the static friction between the threadbar and the self-swelling cartridges. As the rock mass deformation increases further, the tensile force of the bolt increases and the bolt starts to slide in the anchorage cartridges and the bolt enters the sliding deformation stage.

Figure 2b shows that in the sliding deformation stage, the axial force is higher than the static friction resistance between the threadbar and the anchorage cartridges. The bolt de-couples from the self-swelling cartridges and slides. At the same time, the sliding piston slides and enters the sliding-resistance cone pipe. The sliding resistance increases gradually due to the constraint provided by the cone pipe wall. The sliding-resistance cone pipe is blocked by the self-swelling compound of the anchorage section and it cannot move; however, it can undergo plastic deformation due to the extrusion force from the sliding piston and the nut.

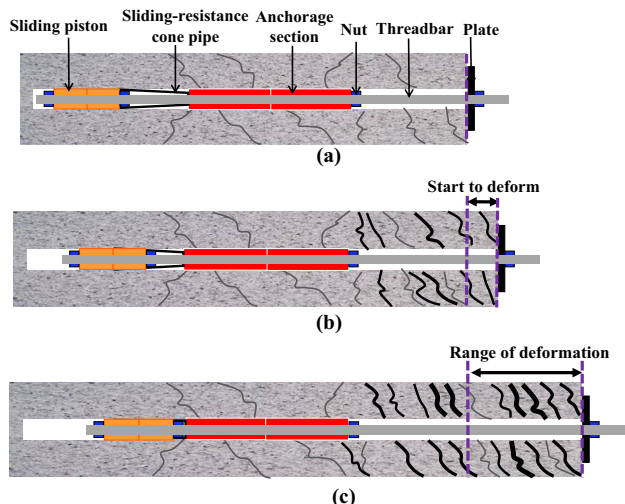


**Fig. 2** Schematic diagrams of a 2S-bolt in operation: **a** initial deformation stage; **b** frictional sliding stage; **c** steel stretching stage

The load of the 2S-bolt during the sliding deformation stage is controlled by the resistance to the sliding piston by the cone pipe, and the deformation amount is restricted by the length of the cone pipe. The shape of the cone pipe is dimensioned such as the sliding force of the bolt is lower than the yield load of the threadbar. Once the sliding piston has reached the end of the cone pipe, the sliding deformation stage ends and the steel stretching deformation stage starts.

Figure 2c illustrates that as the sliding piston reaches the end of the cone pipe, it will be locked in place. Further rock mass deformation will cause the load in the threadbar to increase and reach the yield load of the bolt. The bolt will deform plastically purely by steel stretching of the threadbar until its ultimate plastic deformation capacity is reached.

For this bolt to work as intended in the first deformation stage, the self-swelling cartridges in the anchorage section must be in close contact with the borehole wall. The threadbar must be able to slide relative to the self-swelling cartridges in the anchorage section. In addition, the load in the threadbar when it slides in the self-swelling cartridges should be close to but smaller than the yield load of the threadbar. The following force relation is required for a functional 2S-bolt:

$$F_{\text{cartridge - borehole}} > F_{\text{yield load}} \geq F_{\text{cartridge - threadbar}} \quad (1)$$

where  $F_{\text{cartridge-borehole}}$  is the frictional force between the self-swelling cartridges and the borehole wall,  $F_{\text{cartridge-threadbar}}$  is the frictional force between the self-swelling cartridges and the threadbar, and  $F_{\text{yield load}}$  is the yield load of the threadbar.

In the frictional sliding stage, the frictional force between the self-swelling cartridges and the borehole wall must be higher than the resistance force of the sliding piston as it enters the sliding-resistance cone pipe. This is necessary to prevent the cone pipe from sliding. Therefore, the following force relation is required:

$$F_{\text{cartridge - borehole}} > F_{\text{piston - cone pipe}} \quad (2)$$

where  $F_{\text{piston-cone pipe}}$  is the slip-resistance force of the sliding piston as it enters the sliding-resistance cone pipe.

In the steel stretching stage, the anchor force of the self-swelling cartridges with the borehole wall needs to be higher than the ultimate load of the threadbar to ensure that the bolt will not fail due to slippage. As a result, we have

$$F_{\text{cartridge - borehole}} > F_{\text{ultimate load}} \quad (3)$$

where  $F_{\text{ultimate load}}$  is the ultimate load of the threadbar.

To ensure that these relations are satisfied, it is necessary to accurately measure (a) the sliding resistance between the threadbar and the self-swelling cartridges, (b) the frictional force between the self-swelling cartridges and the borehole wall, and (c) the slip resistance force between the sliding piston and the cone pipe. A detailed laboratory study was

conducted to test the behaviors of each component of the 2S-bolt and the results are presented in the next section.

### 3 Tests of Components of 2S-Bolt

#### 3.1 Test Plan

To study the working mechanism of the 2S-bolt, it is necessary to measure the sliding resistances of the three components of the bolt accurately, which leads to three tests: (1) test of friction between the threadbar and the self-swelling cartridges, (2) test of friction between the self-swelling cartridges and the borehole wall, and (3) test of friction between the sliding piston and the cone pipe. The testing scheme is shown in Table 1. For these tests, different lengths of the self-swelling cartridges varying by a 150 mm increment were used.

To test the interface friction resistance between the threadbar and the self-swelling cartridges, the cartridges are restrained by flanges at both ends of a simulated borehole using split-steel tubes and a force is applied to the bolt, as shown in Fig. 3a. When testing the frictional resistance between the self-swelling cartridges and the borehole wall, nuts and gaskets are used to restrain both ends of the cartridges and a force is applied to the threadbar to force the cartridges to slide inside the simulated borehole, as shown in Fig. 3b. When testing the frictional resistance of the sliding piston as it enters the cone pipe, a flange is fixed on one side of the simulated borehole and a force is applied to the bolt to pull the piston into the pipe, as shown in Fig. 3c.

#### 3.2 Test Samples

The 20 mm diameter threadbar used for the test is made of a manganese-steel alloy with a yield load capacity of 165 kN and an ultimate load capacity of 210 kN. The length, outer diameter, and wall thickness of the cone pipe

are 350, 42, and 1.5 mm, respectively, and the taper is from 30 to 42 mm ( $0.97^\circ$ ). Each cartridge for making the anchorage section and the sliding piston is 150 mm long, with an inner diameter of 23 mm and an outer diameter of 40 mm. The anchorage agent has a density of  $1.6 \text{ g/cm}^3$ . An absorbent sponge is attached to the cartridge wall, which contains some 1 mm diameter holes. Before a test, the cartridges are soaked in water for 8–12 min to initiate the expansion of the anchorage agent.

#### 3.3 Test Setup

The rockbolt pull-test machine, which has a servo-loading controller, is shown in Fig. 4. The load and displacement capacities of the test facility are 300 kN and 800 mm, respectively, and the force and displacement loading rates can be in the ranges of 0.1–50 kN/min and 0–200 mm/min, respectively.

During a test, a pulling force was applied to the bolt by the jack piston. The tests were conducted using displacement-controlled loading at a speed of 15 mm/min. Load and displacement data were recorded respectively by a pressure sensor and a rope-displacement sensor that were connected to an automatic data acquisition system.

As shown in Fig. 5, split-steel tubes with a 50 mm outer diameter and some steel hoops with a 50 mm inner diameter are used to simulate boreholes. The steel hoops are used to restrain the steel tube and increase its stiffness to simulate the field condition.

#### 3.4 Test Results

##### 3.4.1 Frictional Resistance Between the Threadbar and the Self-Swelling Cartridges

In this test, the length of the self-swelling cartridges was varied from 30 to 90 cm with a 15 cm increment. The

**Table 1** Tests of friction resistances between components of the 2S-bolt

Test type	Cartridge length (mm)					
1. Friction between threadbar and self-swelling cartridges	150	300	450	600	750	900
2. Friction between self-swelling cartridges and borehole	150	300	450	600	750	900
3. Friction between sliding piston and cone pipe	0	150	300	450	600	–

**Fig. 3** Schematic diagrams of tests of bolt components: **a** test of friction between threadbar and self-swelling cartridges; **b** test of friction between self-swelling cartridges and borehole wall; **c** test of friction between sliding piston and cone pipe

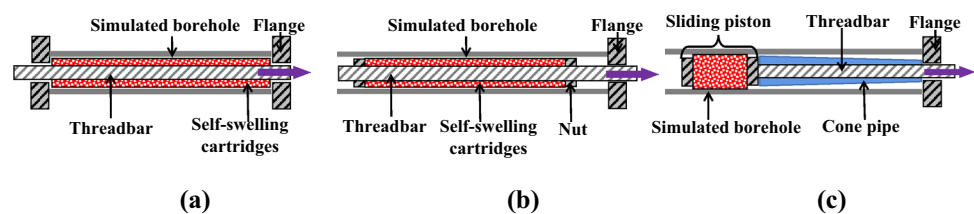




**Fig. 4** Rockbolt pull-out test machine

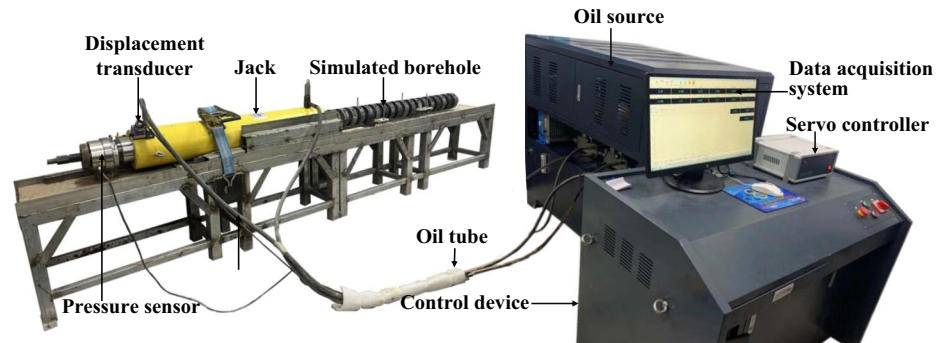
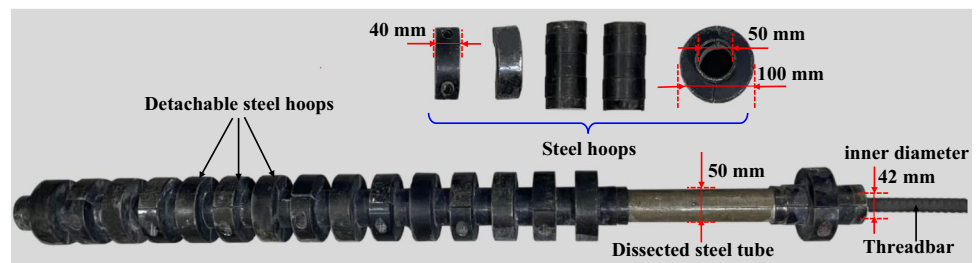


**Fig. 5** Steel tube and hoops used to simulate borehole, with a threadbar installed



load–displacement curves are shown in Fig. 6. No sliding occurred between the cartridges and the borehole wall, and the threadbar was either pulled out of the cartridges or failed in tension.

As the length of self-swelling cartridges increases, the frictional resistance between the threadbar and the cartridges increases. When the lengths of the self-swelling cartridges are 30, 45, 60 and 75 cm, the maximum loads are 29.5, 85.6, 152.5 and 191 kN, respectively. After the peak load is reached, the load drops rapidly and the friction between the bolt and the cartridges decreases gradually as sliding continues. For the case with 90 cm long cartridges, there is no bolt sliding and the threadbar fails in tension after 168 mm of plastic deformation. For the case with 75 cm long cartridges, there is some steel stretching initially but when the load reaches 191 kN, the frictional resistance between the bolt and the cartridges is overcome and bolt sliding occurs thereafter.

The frictional resistance of the 2S-bolt must be close to but lower than its yield load of 165 kN during the initial deformation stage. This is required to avoid plastic deformation of the bolt itself at this stage. Based on the test results, it is seen that a cartridge length of 60 cm can be the anchorage length of the 2S-bolt.

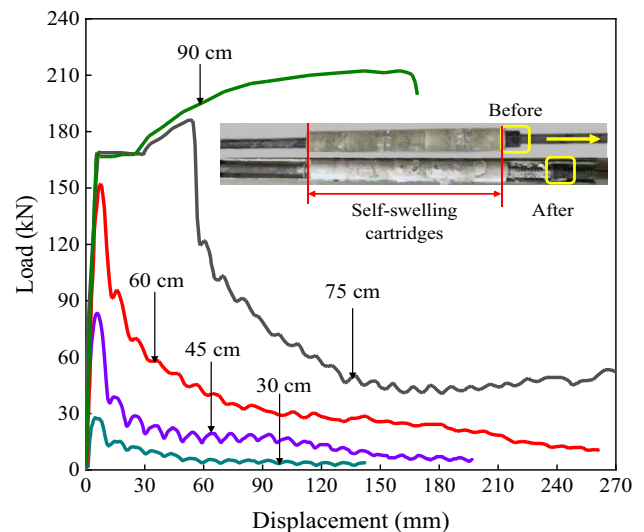


**Fig. 6** Sliding resistance between the threadbar and the cartridges of different lengths

### 3.4.2 Frictional Resistance Between the Self-Swelling Cartridges and the Borehole Wall

The test results for the frictional resistance between the self-swelling cartridges and the borehole wall are shown in Fig. 7. As the cartridge length increases, the frictional

resistance between the cartridges and the borehole wall increases. When the lengths of the cartridges are 15, 30, and 45 cm, the maximum loads are 90, 156, and 192 kN, respectively. The load decreases rapidly post the maximum load due to the sliding of the cartridges relative to the borehole wall. When the cartridge length is 60 cm, the load reaches a maximum of 210 kN and the threadbar fails in tension.

The anchor force between the cartridges and the borehole wall must be higher than the ultimate load capacity of the bolt so that there is no sliding between the anchorage agent and the borehole wall. Therefore, 60 cm cartridge length is used for the anchorage section of the 2S-bolt.

### 3.4.3 Piston Sliding Resistance Test

The load–displacement curves for pistons of different lengths sliding in the cone pipe (350 mm in length with diameters of the large and small openings of 42 and 30 mm, respectively) are shown in Fig. 8. When the length of the sliding piston is 0 cm, i.e., there is no cartridge and only a nut in the piston section, the slip displacement increases steadily as the load increases and then the load decreases after a peak load of 69 kN is reached. When the lengths of the piston are 15 and 30 cm, the loads show an overall trend of increase with the increase of displacement until the peak loads are reached, and then the loads decrease. When the piston length is 45 cm, there is a small drop of the load after the first peak load of 186 kN, and then the load continues to increase when the displacement reaches 360 mm and the test is stopped. When the length of the piston is 60 cm, the load–displacement curve indicates that there is no piston sliding and the threadbar breaks in tension.

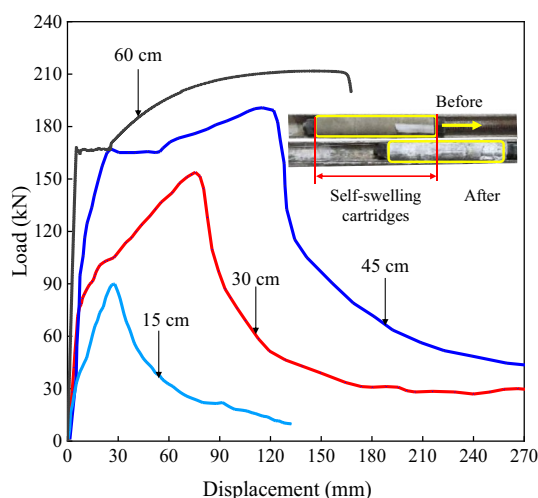


**Fig. 7** Load–displacement curves with different cartridge lengths obtained from the tests of frictional resistance between the cartridges and the borehole wall

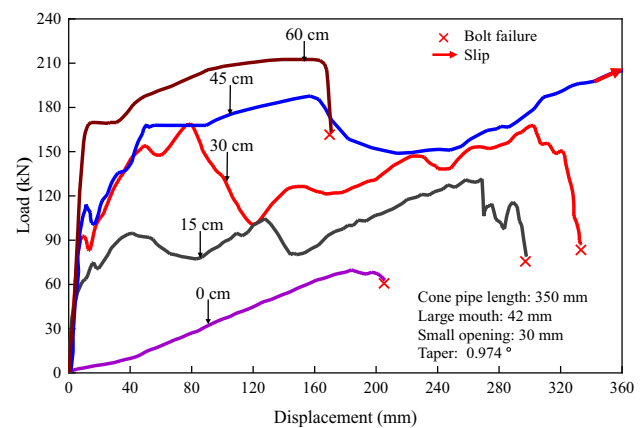


**Fig. 8** Load–displacement curves for pistons of different lengths sliding in 350 mm long cone pipe

It is seen that by adjusting the length of the sliding piston that enters the cone pipe, high load resistance with large deformation can be achieved.

After the tests, the conditions of the cone pipes were examined. As shown in Fig. 9, plastic deformations of the pipes were resulted from the sliding of the piston.

### 3.5 Prediction of Slip Resistance and Elongation

As shown in Fig. 10, the slip resistance force between the self-swelling cartridges and the borehole wall is significantly higher than the frictional force between the threadbar and the self-swelling cartridges, especially when the anchorage length is short.

For the 60 cm long cartridge case, the interface between the cartridges and the borehole wall provides a frictional resistance force higher than the ultimate load of the threadbar (210 kN). However, because the bolt failed at 210 kN, the actual friction force between the cartridge and the borehole wall could not be known in this case. The frictional resistance force between the threadbar and the cartridges is close to the yield load of 152.1 kN when the anchorage length is 60 cm. Therefore, when the length of the self-swelling cartridges is 60 cm, the threadbar can slide in

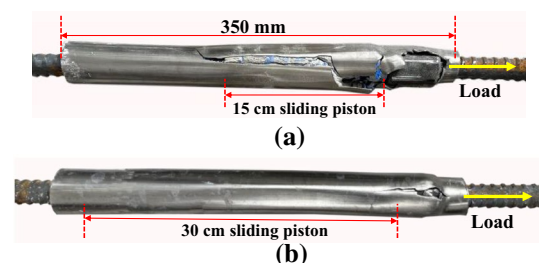


**Fig. 9** Post-test photos of pistons and cone pipes: **a** 15 cm sliding piston; **b** 30 cm sliding piston

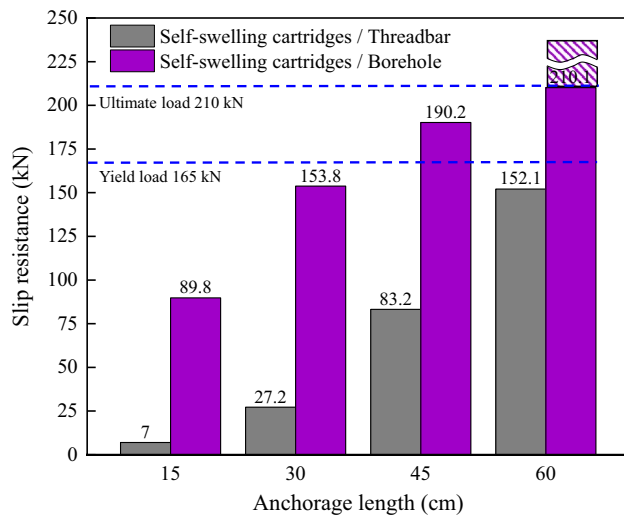


**Fig. 10** Relations between interface slip resistance forces and anchorage length

the cartridge while the cartridge and borehole wall remain securely attached.

During the elastic loading stage, the anchor force is controlled by the frictional force between the threadbar and the anchorage cartridges. Once the bolt begins to slide, the sliding resistance force is controlled by the piston sliding in the cone pipe. After the sliding deformation of the bolt is exhausted, the piston is locked in place and the threadbar deforms by steel stretching until it breaks.

Based on the above test results of the components of the 2S-bolt, we can imagine the load–displacement curve of a bolt with 60 cm long cartridges and a 30 cm long piston, by combining the tests results shown in Sects. 3.4.1–3.4.3, and the curve is presented in Fig. 11. The curve is composed of three parts. From 0 to 6.8 mm displacement, the load increases and reaches the initial peak load of 152.1 kN. The threadbar starts to slide in the cartridges and the load

decreases to about 91.4 kN at a displacement of 13.8 mm. In the displacement range between 13.8 and 308.5 mm, the sliding piston travels in the cone pipe. The load increases initially and reaches 168 kN at a displacement of about 85.3 mm. Then, the load decreases to about 100 kN at a displacement of 125 mm. This behavior is believed to be caused by the shape difference between the sliding piston and the cone pipe. From 125 to 308.5 mm, the load increases due to growing resistance from the compaction of the cartridge material. From 308.5 to 473.2 mm, the behavior represents a typical tensile test curve of steel, which means that the piston is locked in place and the threadbar deforms by steel stretching. In our study, actual tests of assembled 2S-bolts were conducted and the test results are presented in the next section.

#### 4 Tests of Assembled 2S-Bolts

Five 2S-bolts were made, each with an anchorage cartridge length of 60 cm and a piston length of 0, 15, 30, 45, or 60 cm. The length of the cone pipe in all bolts is 350 mm, and the larger and smaller inner diameter of the pipe are 42 and 30 mm, respectively. The materials used in the experiment are consistent with those described in the previous section. The bolts were tested using static pull-out test and the test results are shown in Fig. 12. When the piston length is either 0 or 15 cm, the sliding resistance force is low during piston sliding and the load increases rapidly when the piston reaches the end of the cone pipe. Steel stretching follows and the bolt breaks after reaching the peak load of 210 kN. The deformations are large, which are 618.8 and 573.8 mm for 0 and 15 cm piston lengths, respectively.

When the piston length is 30 cm, the load increases from 102.5 to 165 kN in the piston sliding stage. The piston is locked in place at a displacement of 226 mm, followed by

**Fig. 11** Imagined typical load–displacement curve of 2S-bolt (piston length 30 cm, anchorage length 60 cm)

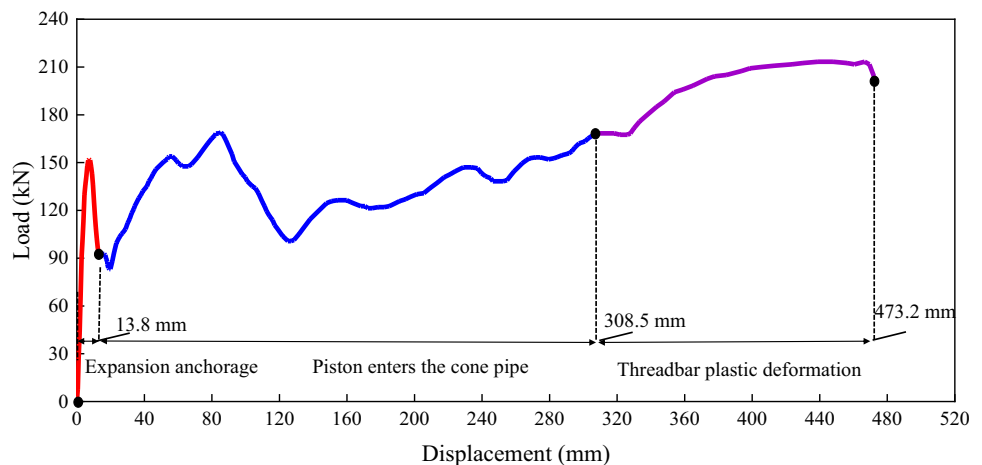
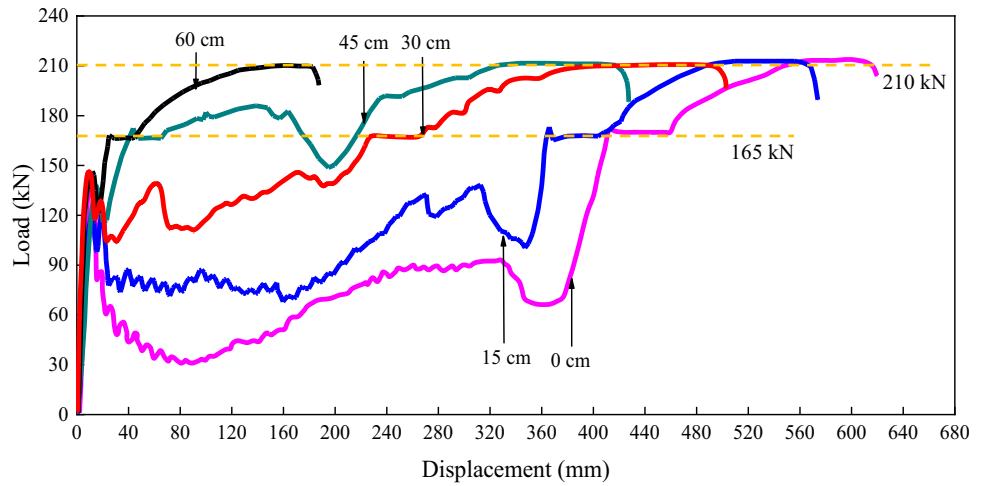




**Fig. 12** Load–displacement curves of 2S-bolts with different piston lengths (60 cm long anchorage cartridge length and 35 cm long cone pipe)



steel stretching and the maximum load and deformation are 210 kN and 502.8 mm, respectively.

When the piston length is 45 cm, the threadbar starts to slide at a displacement of 20.1 mm; the load decreases initially and then increases rapidly from displacements 20.1–40 mm during the initial sliding of the piston. The threadbar starts to deform plastically, and once the load reaches 183 kN the piston starts to slide again and the load decreases briefly, followed by a continuous increase until the bolt breaks at a displacement of 427.5 mm.

When the piston length is 60 cm, there is only a slight decrease of load due to the sliding of the threadbar in the cartridges and there is no piston sliding. The bolt deforms plastically starting at 24.5 mm and breaks after a deformation of 187.5 mm.

To evaluate the mechanical properties and energy absorption characteristics of the 2S-bolt, the deformation, average load, absorbed energy, and energy absorption rate (EAR)

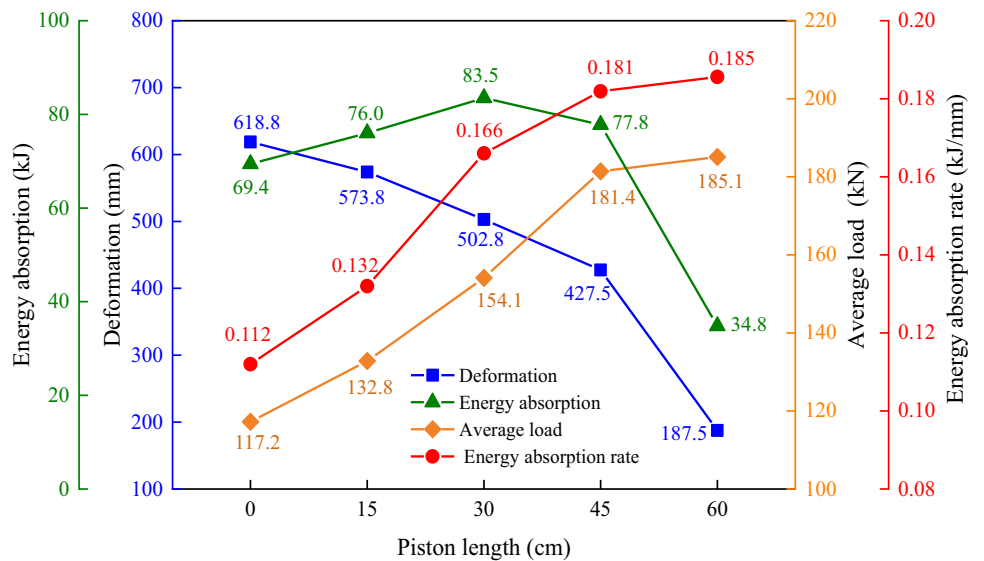
for each piston length are plotted in Fig. 13. As shown in Eq. (4), the EAR, which is defined as the total absorbed energy divided by the total displacement of the bolt, reflects the average energy absorption capacity per unit length.

$$EAR = \int_0^L F(l)dl/L \tag{4}$$

where  $F(l)$  is the slip resistance load and  $L$  is the total displacement of the bolt.

Figure 13 shows that the deformation capacity of the bolt decreases as the piston length increases. As the piston length increases from 0 to 45 cm, the deformation capacity decreases from 618.8 to 427.5 mm. For a piston length of 60 cm, the deformation capacity is 187.5 mm, which is the lowest. The energy absorption capacity initially increases and then decreases as the piston length increases. The

**Fig. 13** Relations between load, deformation, energy absorption, EAR and piston length



maximum and minimum energy capacities are 83.5 and 34.8 kJ for piston lengths of 30 and 60 cm, respectively.

Both the average load and the average energy absorption rate increase with the increase of piston length. When the piston length is increased from 30 to 45 cm, the average load and energy absorption rate increase 17.7% and 9.0%, respectively. When the piston length is increased from 45 to 60 cm, the average load increases only 2.0% and the energy absorption rate increases only 2.2%.

As the piston length increases, the load capacity increases while the deformation capacity decrease. Because energy is the product of load and displacement, an optimal piston length of 30 cm is found to have the maximum energy absorption capacity (83.5 kJ) of the bolt. For applications that requires a large load capacity in addition to large deformation capacity, a piston length of 45 cm can be considered.

## 5 Discussions

### 5.1 Stages of Deformation of 2S-Bolt

Two load–displacement curves are shown in Fig. 14. One is obtained by combining the test results of segments and the other by direct loading of an assembled 2S-bolt. Both agree with each other well. Based on the test results, the load–displacement curve of a 2S-bolt can be divided into four stages: static, decoupling, piston sliding, and steel stretching stages. During the static deformation Stage I, the load is controlled by the bond stress between the threadbar and the anchorage cartridges and the piston remains stationary. Once the force reaches the maximum static frictional force between the bolt and the self-swelling cartridges, the state changes from the static friction state to a dynamic friction state with a slight decrease of the load due to debonding of the threadbar from the anchorage agent in Stage II. The load is controlled by the movement of the piston during piston sliding in Stage

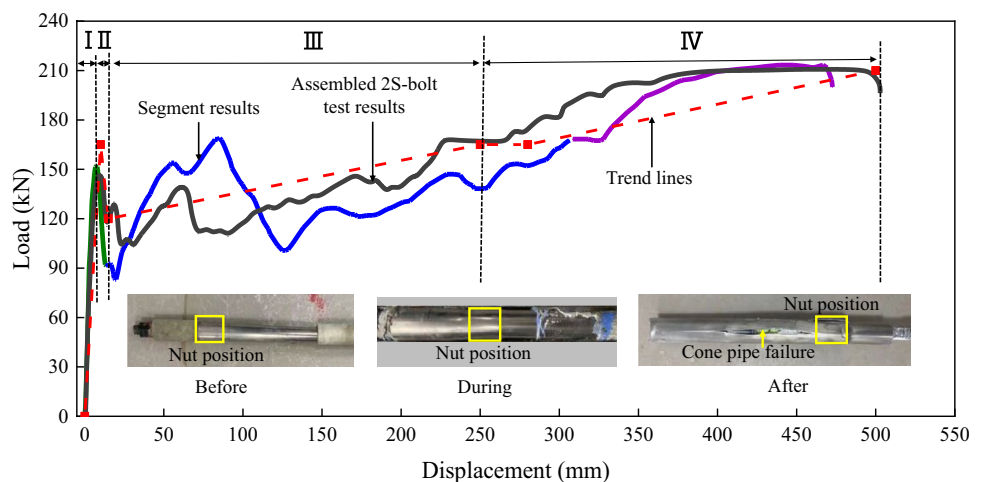
III. When the piston enters the cone pipe, the resistance force generally increases with the increase of deformation. The fluctuation of the load is caused by the extrusion frictional force between the piston and the cone pipe wall. The load increases to the yield load of 165 kN at a displacement of about 200–300 mm. Once the load reaches the yield load, the bolt enters the steel stretching Stage IV. The load increases due to strain-hardening of the threadbar and it breaks shortly after the peak load of 210 kN is reached. It should be noted that in the steel stretching stage, plastic deformation of the steel is the dominant form of deformation of the bolt although there is also a small amount of piston sliding as the agent is further compressed. The cone pipe is steadily squeezed by the sliding piston, which can result in tensile cracks in the pipe, as shown in the right photo insert in Fig. 14.

The sliding-resistance cone pipe solves the problem of decreasing frictional resistance when the deformation amount is large for conventional friction bolts. It allows the sliding resistance to increase during deformation. Coupled with the later stage strain-hardening of the steel, the bolt provides increasing load resistance and large deformation capacity for rock support, which is illustrated by the trend lines shown in Fig. 14.

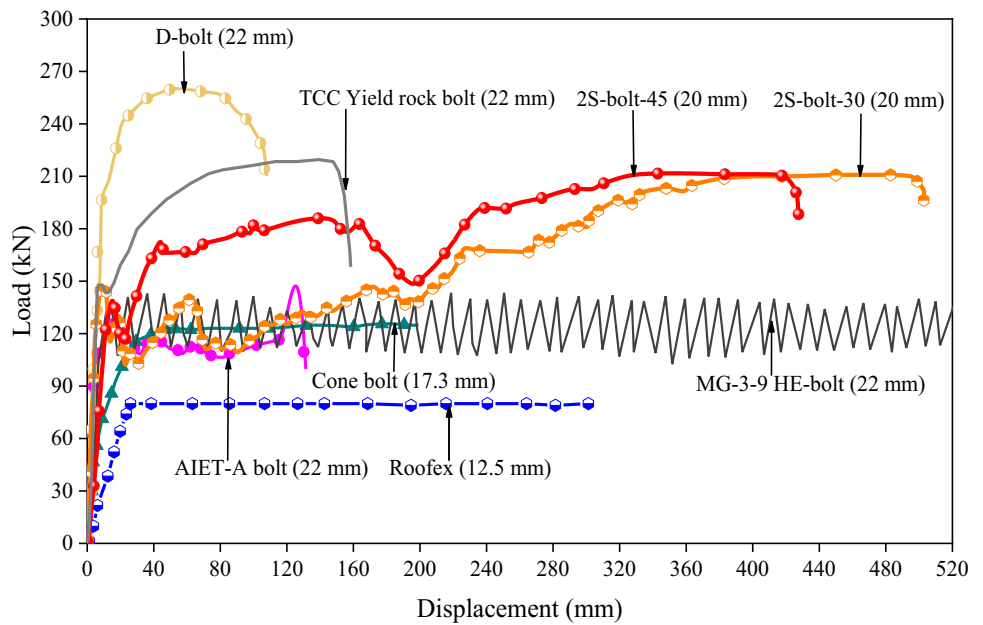
### 5.2 Comparison of Mechanical Properties of 2S-Bolt with Other Energy-Absorbing Bolts

Figure 15 compares the load–displacement curves of two 2S-bolts with those of some other rockbolts. D-bolt (22 mm diameter) and TCC (tension and compression-coupled) Yield rockbolt (22 mm diameter) (Wu et al. 2019), which rely on steel stretching to absorb energy, have load and displacement capacities of 260 kN and 108 mm and 220 kN and 158 mm, respectively. The average load capacity of He-bolt (22 mm diameter) is about 125 kN and the displacement capacity is up to 1000 mm. The peak load of conebolt

**Fig. 14** Load–displacement curves of 2S-bolt



**Fig. 15** Load–displacement curves of 2S-bolts and some other bolts (curve data from Hao et al. 2020)



(17.3 mm diameter) is about 190 kN, with a displacement capacity of 500 mm. The axial splitting bolt (AIEA-T bolt, 22 mm diameter) can provide about 120 kN load resistance during the process of splitting and sliding of the energy-absorbing component; however, the displacement capacity is determined by the length of the external energy-absorbing component. The 2S-bolt with a 30 cm long sliding piston can increase the resistance force from 120 to 210 kN, deform up to 502.8 mm, and absorb 83.5 kJ energy. The 2S-bolt with a 45 cm long sliding piston can deform up to 427.5 mm and absorb 77.8 kJ energy with an average load capacity of 181.7 kN.

It is seen that the 2S-bolt has a larger deformation capacity than bolts that rely purely on steel stretching to absorb energy. It also has a higher load capacity than other friction bolts. A 2S-bolt utilizes both frictional sliding and steel stretching effectively to absorb energy.

### 5.3 Cost Analysis of 2S-Bolt

A cost analysis of the 2S-bolt is conducted and the results are shown in Table 2. The cost of a 15 cm long self-swelling

cartridges is US\$0.50. The cost of a 35 cm long cone pipe is \$3.20, and the cost of a 2.2 m long threadbar (20 mm diameter) is \$5.20. The total cost of a 2S-bolt depends on the length of the cartridges used for the piston and the anchorage and a few examples are listed in Table 2. For a 2S-bolt with a 30 cm long sliding piston and a 60 cm anchorage length, the cost is \$13.6.

As for other types of rock bolts, installation cost will vary depending on the end-users, and therefore is not included in the cost analysis above.

## 6 Conclusion

A new rockbolt named 2S-bolt, which is composed of a threadbar, a cone pipe, an anchorage section and a sliding piston, is developed in this study. When the sliding piston is sliding in the cone pipe, frictional sliding with load increase is realized. When the piston locks in place in the cone pipe, plastic deformation of the steel bar takes place. This combination of frictional sliding and steel stretching results in a

**Table 2** Cost analysis of an 2S-bolt

Anchorage agent cost (USD)	Sliding piston cost (USD)	Threadbar cost (USD)	Face plate cost (USD)	Nut cost (USD)	Cone pipe cost (USD)	Total cost (USD)
2.0	0	5.2	1.2	0.5	3.2	12.1
2.0	0.5	5.2	1.2	0.5	3.2	12.6
2.0	1.0	5.2	1.2	0.5	3.2	13.1
2.0	1.5	5.2	1.2	0.5	3.2	13.6
2.0	2.0	5.2	1.2	0.5	3.2	14.1

rockbolt with a high load capacity and a large deformation capacity.

The initial anchor force of the bolt can be adjusted by changing the length of the anchorage section, and the sliding resistance force can be controlled by adjusting the length of the sliding piston. The results of the static pull-out tests show that the bolt with a 30 cm long sliding piston can increase the load from 120 to 210 kN and it has a deformation capacity and an energy absorption capacity of 502.8 mm and 83.5 kJ, respectively. The average anchor force of the bolt with a 45 cm long sliding piston is 181.7 kN with an energy absorption capacity of 77.8 kJ.

Compared with some existing energy-absorbing bolts, the new bolt can absorb a large amount of energy at a higher load capacity, which is beneficial for rock support. The installation of a 2S-bolt is simple and the unit cost is low. It is envisioned that the 2S-bolt has the potential for application in squeezing and rockbursting grounds.

**Acknowledgements** This study was funded by the National Science Foundation of China (51874068, 52074062, 51974061, 42177169).

**Data availability** All data used during this study are available from the corresponding author by request.

## Declarations

**Conflict of Interest** The authors declare that they have no known competing financial interests or personal relationships that could have appeared to influence the work reported in this paper.

## References

- Ansell A (2005) Laboratory testing of a new type of energy absorbing rock bolt. *Tunn Undergr Space Technol* 20(4):291–300
- Cai M (2019) Rock support in strainburst-prone ground. *Int J Min Sci Technol* 29(4):529–534
- Cai M, Champaigne D (2012) Influence of bolt-grout bonding on MCB conebolt performance. *Int J Rock Mech Min Sci* 49:165–175
- Cai M, Kaiser P (2018) Rockburst support reference book—volume I: rockburst phenomenon and support characteristics, p 284
- Cai M, Kaiser PK (2022) Selecting the ‘right’ rockbolts for burst-prone drifts. *RaSim10, SME*, p 13
- Cai M, Champaigne D, Coulombe JG, Challagulla K (2019) Development of two new rockbolts for safe and rapid tunneling in burst-prone ground. *Tunn Undergr Space Technol* 91:103010
- Dai LP, Pan YS, Wang AW (2018) Study of the energy absorption performance of an axial splitting component for anchor bolts under static loading. *Tunn Undergr Space Technol* 81:176–186
- Dai LP, Pan YS, Li ZH, Wang AW, Xiao YH, Liu FY, Shi TW, Zheng WH (2021) Quantitative mechanism of roadway rockbursts in deep extra-thick coal seams: theory and case histories. *Tunn Undergr Space Technol* 111:103861
- Hao Y, Wu Y, Ranjith P, Zhang K, Hao G, Teng Y (2020) A novel energy-absorbing rock bolt with high constant working resistance and long elongation: Principle and static pull-out test. *Constr Build Mater* 243:118231
- He MC, Gong WL, Wang J, Qi P, Tao ZG, Du S, Peng YY (2014) Development of a novel energy-absorbing bolt with extraordinarily large elongation and constant resistance. *Int J Rock Mech Min Sci* 67:29–42
- Hoek E, Kaiser PK, Bawden WF (1995) Support of underground excavations in hard rock. A. A. Balkema, Rotterdam
- Jager A (1992) Two new support units for the control of rockburst damage. In: International symposium on rock support, pp 621–631
- Kaiser PK, Cai M (2012) Design of rock support system under rockburst condition. *J Rock Mech Geotech Eng* 4(3):215–227
- Kang H, Wu Y, Gao F, Lin J, Jiang P (2013) Fracture characteristics in rock bolts in underground coal mine roadways. *Int J Rock Mech Min Sci* 62:105–112
- Khaleghparast S, Aziz N, Remennikov A, Anzanpour S (2023) An experimental study on shear behaviour of fully grouted rock bolt under static and dynamic loading conditions. *Tunn Undergr Space Technol* 132:104915
- Knox G, Berghorst A (2019) Dynamic testing: determining the residual dynamic capacity of an axially strained tendon. In: Ground support 2019: proceedings of the ninth international symposium on ground support in mining and underground construction. Australian Centre for Geomechanics, pp 231–242
- Li CC (2010) Field observations of rock bolts in high stress rock masses. *Rock Mech Rock Eng* 43(4):491–496
- Li CC, Doucet C (2012) Performance of D-bolts under dynamic loading. *Rock Mech Rock Eng* 45(2):193–204
- Li D, Ma S, Lane M, Chang P, Crompton B, Hagen SA (2023) Laboratory investigations into the failure mechanisms of new yielding and inflatable rockbolts under axial and shearing loading conditions. *Rock Mech Rock Eng* 56(1):565–587
- Masoudi R, Sharifzadeh M (2018) Reinforcement selection for deep and high-stress tunnels at preliminary design stages using ground demand and support capacity approach. *Int J Min Sci Technol* 28(4):573–582
- Ortlepp WD (2000) Observation of mining-induced faults in an intact rock mass at depth. *Int J Rock Mech Min Sci* 37(1):423–436
- Srivastava LP, Singh M (2015) Effect of fully grouted passive bolts on joint shear strength parameters in a blocky mass. *Rock Mech Rock Eng* 48(3):1197–1206
- Varden R, Lachenicht R, Player J, Thompson A, Villaescusa E (2008) Development and implementation of the garford dynamic bolt at the Kanowna Belle Mine. In: 10th Underground operators' conference—boom and beyond, pp 95–104
- Wang G, Wu XZ, Jiang YJ, Huang N, Wang SG (2013) Quasi-static laboratory testing of a new rock bolt for energy-absorbing applications. *Tunn Undergr Space Technol* 38:122–128
- Windsor CR, Thompson AG (1992) A new friction stabilizer assembly for rock and soil reinforcement applications, Paper presented at the International symposium on rock support, pp 523–529
- Wu X, Jiang Y, Wang G, Gong B, Guan Z, Deng T (2019) Performance of a new yielding rock bolt under pull and shear loading conditions. *Rock Mech Rock Eng* 52(9):3401–3412
- Xu S, Hou PY, Li RR, Cai M (2021) An experimental study on the mechanical properties and expansion characteristics of a novel self-swelling cartridge for rock breakage. *Rock Mech Rock Eng* 54(2):819–832

**Publisher's Note** Springer Nature remains neutral with regard to jurisdictional claims in published maps and institutional affiliations.

Springer Nature or its licensor (e.g. a society or other partner) holds exclusive rights to this article under a publishing agreement with the author(s) or other rightsholder(s); author self-archiving of the accepted manuscript version of this article is solely governed by the terms of such publishing agreement and applicable law.